A Label-Free Porous Alumina Interferometric Immunosensor

Sara D. Alvarez,[†] Chang-Peng Li,[‡] Casey E. Chiang,[‡] Ivan K. Schuller[‡] Michael J. Sailor[†,*]

[†]Department of Chemistry and Biochemistry and [‡]Physics Department, University of California, San Diego, La Jolla, California 92093

ABSTRACT Anodization of Al is used to produce optically smooth porous alumina (Al_2O_3) films with pores ~60 nm in diameter and ~6 μm deep. The capture protein, protein A, is adsorbed to the pore walls by noncovalent, electrostatic interactions, and thin film interference spectroscopy is used to detect binding of immunoglobulin (IgG). The porous alumina films are stable against corrosion and dissolution in aqueous media at pH 7, allowing quantitative monitoring of steady-state and time-resolved biomolecular binding. The bare porous Al_2O_3 surface displays a significantly greater affinity for protein A than for IgG. The known species specificity of protein A binding to IgG is confirmed; the protein-A-modified sensor responds to IgG derived from rabbit, but not chicken (IgG/IgY). A "cascaded", or multiprobe sensing approach, is demonstrated, in which a specific target, sheep IgG, is administered to a sample modified with a protein A/rabbit anti-sheep IgG assembly. Binding measurements are confirmed by fluorescence microscopy using fluorescein-labeled IgG.

KEYWORDS: porous alumina · label-free · immunosensor · biosensor · interferometry

Label-free biosensors are important for medical,[1] environmental monitoring,[2] and biochemical research applications.[3] A label-free biosensor incorporates a specific recognition element, such as an antibody, with a material that possesses an optical,[4] acoustic,[5] or electrochemical[6] response that converts the analyte binding event into a quantifiable signal. A very sensitive optical method is reflectometric interference spectroscopy (RIfS),[7] which is based on white light interference in a thin film. The interference pattern depends on the product of refractive index and thickness, *nL*. Analyte binding to the planar surface of the thin film produces an increase in film thickness (*L*) that produces a shift in the interference pattern measured in the optical spectrum. A proposed route to increase sensitivity of an interferometric sensor is to employ a porous thin film.[8] The porous thin film interferometer relies on a change in average index of refraction (*n*) of a fixed thickness (*L*) layer, rather than on a physical thickness change as with RIfS. While the porous layer still generates an interference pattern, it has a much greater surface area for analyte capture. Analyte binding produces a change in refractive index throughout the film and, consequently, a change in the value of *nL*.[9]

Porous silicon (pSi) and oxidized porous silicon ($pSiO_2$) have been extensively studied as high surface area thin films for label-free biosensing and immunosensing.[10−13] Related work has been initiated in another inorganic porous material, anodic aluminum oxide (pAl_2O_3), for interferometric sensing[14,15] and in planar optical waveguides.[16] Similar to the pSi and $pSiO_2$ systems, the porosity, thickness, and pore diameters of pAl_2O_3 can be tuned by adjusting electrochemical etch conditions,[17] and ordering of pores has been achieved using a double anodization process. The greater stability of Al_2O_3 at physiological pH[18] motivated the present study to investigate the use of pAl_2O_3 for label-free biosensing. Optical biosensing of complementary DNA interactions with pAl_2O_3 has been demonstrated.[14] The system showed excellent sensitivity, although it employed a drying step before quantification. In this work, we demonstrate the first real-time measurements of protein binding in the pAl_2O_3 system, which is important for quantification of kinetic binding measurements[11] and reaction kinetics.[19,20]

RESULTS AND DISCUSSION

Sample Characterization. Anodically etched porous alumina (pAl_2O_3) films form well-ordered cylindrical pores that run continuously through the depth of the film with little to no branching. Figure 1a shows a cross-sectional scanning electron microscope (SEM) image of the porous layer. The average thickness of the films, measured by

See the accompanying Perspective by Walt on p 2876.

*Address correspondence to msailor@ucsd.edu.

Received for review July 18, 2009 and accepted August 24, 2009.

Published online August 31, 2009.
10.1021/nn900825q CCC: $40.75

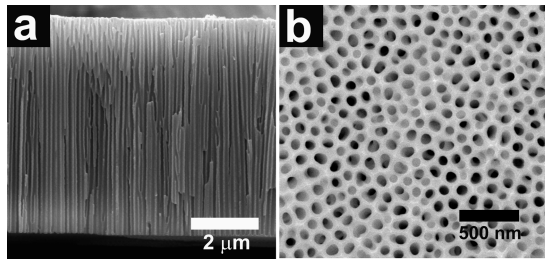

Figure 1. Scanning electron micrographs representative of the porous alumina films used in this study. (a) Cross-sectional view. (b) Plan-view image, showing the entrance to the pores. Average pore diameter is 60 nm, average depth is 6000 nm.

SEM, was 5684 ± 969 nm, in agreement with growth parameters. The diameter of the pore entrance ranged between 48 and 86 nm, with an average pore diameter of 62 nm. The longest dimension of an IgG antibody molecule is 11−17 nm;[23] therefore, the pores in the pAl_2O_3 samples used in this work provide adequate volume to accommodate the biomolecule. The well-defined pore walls display no branching or other obstructions, as are observed in other electrochemically prepared porous systems,[21] making pAl_2O_3 a good material for the sensing of large biomolecules.

Sample thickness and porosity were determined using the spectroscopic liquid infiltration method (SLIM) as previously described.[21] Fitting the optical parameters derived from the reflective interferometric spectra to a Bruggeman effective medium approximation yielded porosity of 39 ± 5% and thickness of 5841 ± 1196 nm. The thickness results obtained from the optical method are in agreement with the above-mentioned SEM measurements.

Detection Method. White light reflection from the porous aluminum oxide films generates a thin film interference spectral pattern (Figure 2). The interference pattern arises from Fabry−Perot interference of light reflecting from the air−porous alumina and the porous alumina−substrate interfaces. The wavelength of the peak maxima in the interference spectrum is governed by the Fabry−Perot relationship:

$$m\lambda = 2nL \quad (1)$$

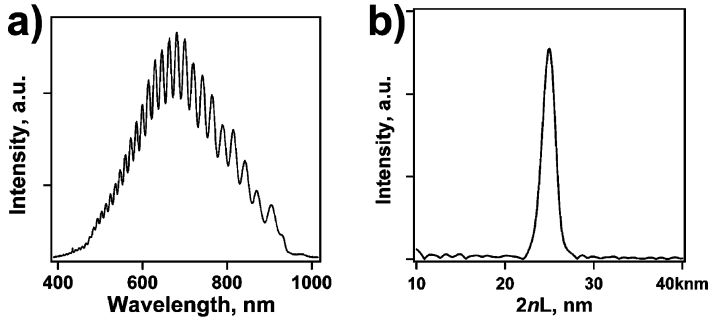

Figure 2. Optical characteristics of a porous alumina thin film. (a) White light reflectance spectrum from a thin film of pAl_2O_3. (b) Fourier transform of the reflectance spectrum in (a) results in a single peak whose position along the *x*-axis corresponds to the effective optical thickness of the thin film, 2*nL*.

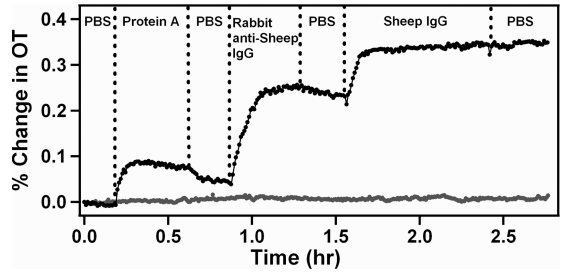

Figure 3. Representative dosing curve for pAl_2O_3 biosensor. The percent change in optical thickness is monitored as a function of time as solutions of protein A, rabbit anti-sheep IgG, and sheep IgG are introduced successively to the flow cell. The upper (black) trace represents the response to solutions of the indicated biomolecules: PBS is a blank solution of aqueous buffer, biomolecule solutions protein A, rabbit anti-sheep IgG, and sheep IgG are present at a concentration of 0.1 mg/mL in PBS. The lower (gray) trace is a control (PBS blank) run on a separate chip. The approximate starting value of optical thickness for the immunosensor sample in PBS was 6837 nm.

where λ is the wavelength of maximum constructive interference for spectral fringe of order *m*, *n* is the mean refractive index of the porous layer and its contents, and *L* is the geometric thickness of the porous layer. The interference pattern changes as a result of any modification in refractive index or thickness of the film as given in eq 1. The right-hand side of the equation (2*nL*) represents the effective optical thickness, which can be obtained from the Fourier transform of the reflectivity spectrum. This analysis has been used to monitor gas adsorption within nanoporous alumina[15,24] and has been applied extensively for sensing in porous Si-based Fabry−Perot films.[9,12,19,25]

The porous framework of pSi films is susceptible to oxidation and hydrolysis in aqueous media,[26] resulting in zero point drift in the sensor response. Thermal oxidation and other chemical treatments[27] can significantly improve the stability of this material; however, degradation remains a problem, and it is often manifested in sensor traces as a drifting baseline.[11] In some cases, the oxidation and hydrolysis phenomena can be harnessed to increase sensitivity,[28−31] although in general such drift is not desirable. In contrast to pSi or $pSiO_2$, pAl_2O_3 is stable in neutral or slightly basic solutions, conditions that are commonly employed in biosensor systems.[18,32]

The stability of the pAl_2O_3 sensor was tested by monitoring the optical thickness in the presence of pH 7.4 PBS buffer in the time scale of a typical biosensor experiment (Figure 3, lower curve). The sensor displays a stable baseline, with no significant decrease in optical thickness due to pAl_2O_3 dissolution.

Immunosensor Experiments. The pAl_2O_3 sample was tested as an immunosensor using a protein A capture probe and two immunoglobulin G (IgG) antibodies. The experiment, represented in Figure 3 and summarized in Table 1, begins with exposure to PBS buffer to saturate the pores and establish a baseline. Then the cap-

TABLE 1. Quantified Changes in Optical Thickness (ΔOT) for Biomolecules Dosed on the Porous Alumina Sensor[a]

capture probe layer	pAl_2O_3 surface modification	biomolecule dosed	Δoptical thickness, nm	% change in OT
1°	none (bare pAl_2O_3 surface)	rabbit IgG	0.52 ± 0.22	0.007 ± 0.003
		sheep IgG	0.80 ± 0.28	0.007 ± 0.003
		protein A	**3.21 ± 1.31**	**0.028 ± 0.016**
2°	pAl_2O_3 + protein A	chicken IgG	0.28 ± 0.95	0.002 ± 0.010
		rabbit anti-sheep IgG	**12.25 ± 2.68**	**0.160 ± 0.050**
		rabbit IgG, F_c portion	5.19 ± 0.45	0.057 ± 0.005
3°	pAl_2O_3 + protein A + rabbit anti-sheep IgG	chicken IgG	0.77 ± 0.68	0.008 ± 0.012
		sheep IgG	**8.27 ± 1.19**	**0.102 ± 0.019**
3°	pAl_2O_3 + protein A + rabbit IgG (F_c portion only)	sheep IgG	0.72 ± 0.85	0.008 ± 0.008

[a]Changes in optical thickness determined from three or more experiments and standard deviations are given. The biomolecules in bold indicate the immunosensor proteins used in Figure 3 and represent positive interactions based on the known affinity of the target molecule.

ture probe, protein A, is adsorbed to the surface. Protein A is derived from *Staphylococcus aureus* bacteria and is part of a small collection of proteins known to bind antibodies in a specific and directional orientation. Since protein A binds the F_c region of an antibody, the antigen binding sites located on the F_{ab} region of the captured antibody are accessible for further binding. The antibody binding affinity of protein A differs depending on the species from which the antibody was derived.[33] Protein A has a strong affinity for IgG derived from rabbits, and this interaction was exploited here to bind rabbit anti-sheep IgG, an antibody developed in rabbits to specifically target IgG from sheep. The reflective interferometric immunosensor was first coated with protein A and then exposed to successive doses of rabbit anti-sheep IgG and sheep IgG.

The protein A capture probe was placed on the pAl_2O_3 surface by physical adsorption. Protein A is negatively charged at pH 7.4,[34] and aluminum oxides are known to strongly adsorb anions on protonated hydroxyl groups or exposed cationic aluminum ions.[35] Upon exposure to a solution of protein A, the percent change in optical thickness increases by approximately 0.1%, corresponding to adsorption of the protein in the porous nanostructure (Figure 3). This value decreases to 0.05% upon rinsing of the sample with PBS buffer, as the free and weakly bound protein is removed. Introduction of rabbit anti-sheep IgG results in an additional increase in optical thickness of 14 nm or 0.20% change in OT, as the antibody becomes specifically bound to the immobilized protein A capture probe. After rinsing with PBS buffer, the percent change in *nL* relative to the protein-A-only value is 0.19%. Finally, introduction of sheep IgG produces an additional 0.12% increase in optical thickness, attributed to binding of sheep IgG to the immobilized rabbit anti-sheep IgG. A final PBS rinse shows no significant decrease in optical thickness, which we attribute to the strong interaction between the two antibodies.

Control Immunosensor Experiments. Several control experiments were performed confirming that the optical thickness changes observed in Figure 3 are due to specific binding interactions between the biomolecules and not due to nonspecific adsorption. The experiments are presented in Figure 4 and summarized in Table 1. The illustration to the left of each set of binding curves in Figure 4 depicts the binding interactions hypothesized to occur within the pAl_2O_3 nanostructure. The first control (Figure 4a) compares the percent Δ*nL* trace observed upon introduction of protein A to a bare pAl_2O_3 sample with the response observed when rabbit antibody is introduced to a bare pAl_2O_3 sample. While rabbit IgG is approximately 3 times larger in mass than protein A (150 *vs* 42 kDa), the increase in optical thickness observed with rabbit IgG is negligible. The result indicates that IgG exhibits a relatively small affinity for pAl_2O_3 compared with the affinity of protein A for this surface. Other studies have shown that IgG can adsorb to alumina films directly;[36] the present result indicates that this interaction is fairly weak at pH 7.4. The surface of pAl_2O_3 can be modified to increase its hydrophobicity,[37,38] which increases the extent of IgG adsorption. However, this approach can lead to denaturation of the antibody and loss of binding activity. The approach used in the present work, involving use of a protein A capture probe to increase the binding of IgG and to properly orient the antibody for subsequent immunosensing, has been successfully demonstrated with porous SiO_2 optical sensors.[9,39]

It should be pointed out that the approach of using protein A to immobilize an IgG capture probe requires the nanosensor to possess a significant volume in which the sensing event can be detected. For example, this approach would be less successful for surface plasmon resonance (SPR) and other sensors that display a distinct decline in sensitivity as the capture probe is placed further from the active sensing surface. Porous optical biosensors like pSi, $pSiO_2$, and the pAl_2O_3 sensor used in the present work respond to refractive index changes that occur within the volume of the porous matrix. Thus they are amenable to such "cascaded", or multiprobe, sensing approaches. A primary limitation of these volume sensors is the size of the pores—the pores must be large enough to admit the capture probe assembly, but they cannot be so large that they scatter the light of the probe optics. The fidelity of the optical interfer-

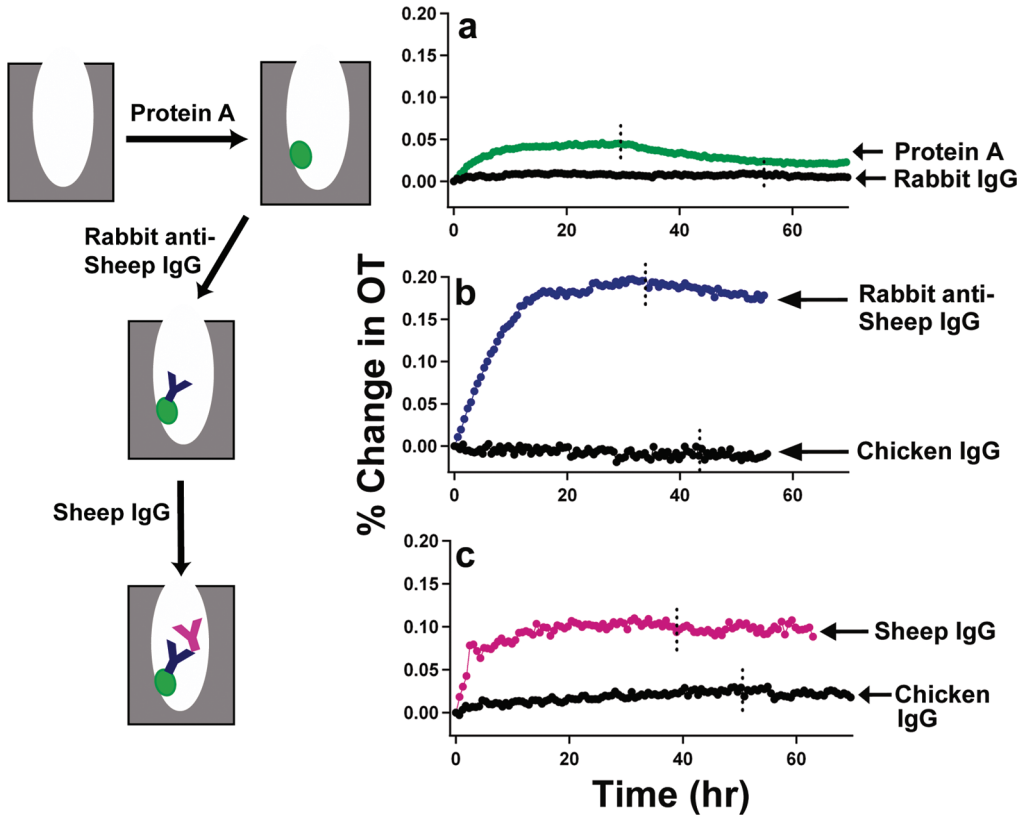

Figure 4. Experiments demonstrating specific binding affinity and controls for the pAl_2O_3 immunosensor. (a) Protein A and rabbit IgG separately dosed on bare pAl_2O_3 sample, demonstrating the greater relative affinity of the surface for protein A. (b) Rabbit anti-sheep IgG and chicken IgG introduced to a protein-A-modified sample. (c) Sheep IgG and chicken IgG introduced to a protein-A-modified sample that contains the protein A + rabbit anti-sheep IgG assembly. The dotted line intersecting each curve designates initiation of a rinse with pure PBS buffer. All biomolecules were introduced at a concentration of 0.1 mg/mL.

ence fringes in the reflectivity spectrum degrades significantly as the pore dimensions approach the wavelength of light, due to the onset of scattering. In addition, the diffusion of IgG can become significantly limited even in pores with diameters much larger than twice the nominal 4 nm hydrodynamic radius of the antibody.[40] Thus, for this type of nanoporous optical biosensor based on antibody interactions, the practical range of pore diameters is probably between 50 and 400 nm, which can be ideally prepared in porous alumina.

Binding of protein A to antibodies is species specific; for example, protein A binds to rabbit and sheep but not to chicken antibodies (IgG/IgY). The black trace in Figure 4b shows that no change in optical thickness is observed when chicken IgG is dosed onto a protein-A-modified pAl_2O_3 sample. Taken with the control run of Figure 4a, this establishes that the observed change in optical thickness when rabbit anti-sheep IgG is dosed onto a protein-A-modified pAl_2O_3 sample is due to a binding interaction with protein A and not due to nonspecific surface adsorption.

The third step in the immunosensor experiment of Figure 3 is to administer a target antigen to the immunosensor. Figure 4c shows the percent increase in optical thickness when the specific target, sheep IgG, is administered to a sample modified with rabbit anti-sheep IgG, whereas chicken IgG produces a negligible response. The rabbit anti-sheep IgG antibody effectively discriminates between the two proteins. The results are summarized in Table 1.

While protein A does not bind chicken IgG, it does have a weak affinity for sheep IgG. Therefore, it is possible that the response measured in the third step, in which sheep IgG is introduced to the protein A + rabbit anti-sheep IgG assembly (shown in Figures 3 and 4c), is due to protein A binding sheep IgG. To test this hypothesis, a rabbit IgG lacking the sheep IgG binding domain was tested on the protein-A-modified surface. The protein used was the F_c domain of rabbit IgG, a truncated antibody containing the binding site for protein A but lacking the F_{ab} fragment needed for antigen binding. Supporting Information Figure 1 presents the dosing profile for this control experiment, and the results are summarized in Table 1. In this case, addition of sheep IgG to the protein A + rabbit IgG (F_c) complex results in no detectable increase in optical thickness. Therefore, it can be concluded that the pAl_2O_3 immunosensor correctly reports the specific interaction occurring between the antibody (rabbit anti-sheep IgG) and its target antigen (sheep IgG).

A tabulation of the steady-state optical thickness changes measured for all of the analytes and controls is presented in Table 1. IgG does not bind significantly to pAl_2O_3 unless the capture protein, protein A, is present on the surface. The immunosensor reports a significant signal only when specific binding interactions are expected (between protein A and IgG, and between the antibody and its antigen).

The extent of binding of sheep IgG to the various modified pAl_2O_3 surfaces was confirmed independently by fluorescence microscopy. Fluorescein isothiocyanate (FITC)-labeled sheep IgG was dosed onto bare pAl_2O_3, pAl_2O_3 containing protein A + rabbit anti-sheep IgG, and pAl_2O_3 containing protein A + the F_c domain of rabbit IgG (Supporting Information Figure 2). The specific binding experiment (pAl_2O_3 containing protein A + rabbit anti-sheep IgG + sheep IgG:FITC) generates a significant fluorescence signal; the surface engineered for specific immunosensing generates fluorescence intensity approximately 50 times greater than all of the controls.

The adsorbed protein A layer appears to significantly suppress nonspecific binding to pAl_2O_3. While previous reports show that IgG binds nonspecifically to alumina surfaces,[36] very little protein adsorption is observed in the present work by fluorescence analysis or by optical interferometry. Once protein A is adsorbed to the surface, the interferometric sensor provides a well-behaved specific binding response while effectively suppressing nonspecific interactions with the surface or with other proteins. The method used in this work to coat the surface with protein A relies on a strong, noncovalent interaction. A more common approach to inhibit nonspecific binding is to chemically attach low affinity molecules such as oligomeric poly(ethylene glycol).[41] Aluminum oxide contains surface hydroxyl groups that are suitable for various coupling reactions, and covalent chemical modification routes[42] have been used to attach peptides,[43] DNA,[44] and poly(ethylene glycol)[41] to pAl_2O_3. Such an approach was not pursued in this work but can be a useful route for expanding the versatility of the material for real-time biosensing of additional biomolecular interactions.

CONCLUSIONS

Thin film interference spectroscopy was used to optically interrogate physical parameters of a 6 μm thick porous alumina film prepared by anodization of aluminum metal. The porous alumina film is stable at physiological pH and shows no significant baseline drift in the time scale of the immunosensor experiments. Changes in refractive index, *n*, of the layer due to replacement of buffer with proteins were monitored during sequential binding of protein A, rabbit anti-sheep IgG, and sheep IgG. The study demonstrated two key issues for label-free biosensors: the preparation of a biological sensing layer that minimizes nonspecific binding and is able to report in real-time sequential addition of multiple large protein analytes.

METHODS

Porous Alumina Fabrication. Porous alumina was fabricated from a 5−8 μm e-beam evaporated aluminum film on n-type silicon using a two-step anodization process. In the first anodization, a 500 nm sacrificial layer of pAl_2O_3 was anodized by application of 60 V in 0.3 M oxalic acid at 5 °C. This first anodization step was used to initialize pore formation and the arrangement of ordered pores. The initial anodized layer was removed with a solution of 5% chromic acid and 3% phosphoric acid. The second anodization was continued using the same conditions until a current drop indicated total anodization of the aluminum film. In order to generate pores of adequate size for admission of the biomolecules, the pores were widened by immersion in room temperature 5% phosphoric acid for 70 min.

Interferometric Reflectance Spectroscopy. Reflectance spectra were obtained from the pAl_2O_3 samples using a tungsten light source and a CCD spectrometer (Ocean Optics, S-2000). The light was directed through a bifurcated fiber optic cable to an optical lens, which focused light on the surface. The optical axis was normal to the plane of the pAl_2O_3 layer. Reflected light was collected through the same lens and directed through the other arm of the bifurcated optical fiber cable to the CCD spectrometer. The wavelength axis of the spectrum from the spectrometer was calibrated using a least-squares fit of five spectral lines observed from a neon lamp, at 585.3, 614.3, 640.2, 703.2, and 811.5 nm. The data spacing of the spectrometer was 0.4 nm. The *x*-axis was inverted, and a linear interpolation was applied such that the data were spaced evenly in units of nm^{-1}. A Hanning window was applied to the spectrum, and it was re-dimensioned to 4096 data points and zero padded to the power of two. A discrete Fourier transform using a multidimensional fast prime factor decomposition algorithm from the Wavemetrics Inc. (www.wavemetrics.com) IGOR program library (FFT) was applied. The Fourier transform of the spectrum yields a peak whose position on the *x*-axis corresponds to the value 2*nL*, or the effective optical thickness of the pAl_2O_3 film.

Characterization of Porous Alumina. Pore size and thickness of the porous films were determined by scanning electron microscopy (SEM) using a FEI Quanta 600 environmental scanning electron microscope operating at an accelerating voltage between 10 and 25 keV. Thickness and porosity of the films were also determined by optical reflectance spectroscopy in which optical thickness changes were monitored upon immersion in organic liquids of known refractive indices, as previously described.[21] The optical thickness of a sample was determined from two different locations on the porous film by measuring the interferometric reflectance spectrum of the film in air and immersed in ethanol, toluene, water, hexane, and acetone having refractive indices of 1.359, 1.494, 1.33, 1.372, and 1.357, respectively. Refractive indices of the liquids were measured using a Milton Roy refractometer. The change in the reflectance spectrum as the medium in the pores is changed from air to the respective liquid was attributed to changes in optical thickness assuming all pores in the film are filled by the solvent. The data were then fit to a two-component Bruggeman effective medium approximation,[21] yielding values for porosity and thickness of the porous alumina layer. The refractive index of the aluminum oxide portion of the film used in the analysis is $n = 1.65$.[22] After porosity and optical thickness measurements, the samples were rinsed with ethanol, dried using a nitrogen stream, and placed in vacuum for at least 15 min prior to the biosensing experiments.

Immunosensor Experiments. Samples were removed from vacuum and placed in a flow cell in which solution was deliv-

ered at a rate of approximately 1 mL/min. A baseline was achieved by dosing phosphate buffered saline solution (PBS, 1× Cellgro brand, Mediatech Inc.) for approximately 20 min. Protein A (EMD Calbiochem) and antibody (IgG) solutions (Jackson Immuno Research Laboratories, Inc.) were delivered by continuously circulating 3 mL of 0.1 mg/mL concentrations (in PBS) of the biomolecules. The flow cell was flushed with PBS solution between biomolecule dosing runs to remove any nonadsorbed or loosely bound proteins within the pores. Data points were collected every 30 s, and each data point represents an average of data obtained over 5 s. The interaction between protein A and the pAl_2O_3 sample is by physical adsorption; therefore, the magnitude of change in optical thickness due to protein A was determined by measuring the optical thickness difference between the initiation of dosing to the baseline reached after the PBS rinse. The magnitude of change in optical thickness due to biomolecular interactions was determined as the change in the value of optical thickness measured just prior to introduction of analyte to the value obtained after the signal reached steady state. In the experiments used to monitor binding of a secondary antibody to the protein A/IgG complex, the sample containing the protein A/IgG assembly was rinsed with PBS for only 15−20 min (in order to minimize removal of bound IgG from within the pores) before addition of the secondary antibody.

Fluorescence Measurements. Immunosensor experiments using fluorescein isothiocyanate (FITC)-labeled sheep IgG were performed in the flow cell setup. At the end of the experiment, the samples were immediately imaged using a fluorescence microscope (Nikon Eclipse LV150) equipped with a CCD camera (Photometrics CoolSNAP HQ2). A 480 ± 20 nm excitation filter and a 535 ± 25 nm emission filter were used. Images were captured on at least three locations on the chip and processed using Metamorph 7.0r4 (Molecular Devices).

Acknowledgment. The authors acknowledge financial support from the Air Force Office of Scientific Research AFOSR-MURI (Grant No. F49620-02-1-0288) and the National Science Foundation under Grant No. DMR-0806859.

Supporting Information Available: Immunosensor binding curve for exposure of F_c domain of IgG to protein-A-modified surface, and subsequent insensitivity toward binding of sheep IgG. Fluorescence analysis of FITC-labeled sheep IgG binding to immunosensor. This material is available free of charge *via* the Internet at http://pubs.acs.org.

REFERENCES AND NOTES

1. Malhotra, B. D.; Chaubey, A. Biosensors for Clinical Diagnostics Industry. *Sens. Actuators, B* **2003**, *91*, 117–127.
2. González-Martínez, M.; Puchades, R.; Maquieira, A. Optical Immunosensors for Environmental Monitoring: How Far Have We Come? *Anal. Bioanal. Chem.* **2007**, *387*, 205–218.
3. Fägerstam, L. G.; Frostell-Karlsson, Å.; Karlsson, R.; Persson, B.; Rönnberg, I. Biospecific Interaction Analysis Using Surface Plasmon Resonance Detection Applied to Kinetic, Binding Site and Concentration Analysis. *J. Chromatogr., A* **1992**, *597*, 397–410.
4. Gauglitz, G. Direct Optical Sensors: Principles and Selected Applications. *Anal. Bioanal. Chem.* **2005**, *381*, 141–155.
5. Länge, K.; Rapp, B.; Rapp, M. Surface Acoustic Wave Biosensors: A Review. *Anal. Bioanal. Chem.* **2008**, *391*, 1509–1519.
6. Grieshaber, D.; MacKenzie, R.; Voros, J.; Reimhult, E. Electrochemical Biosensors—Sensor Principles and Architectures. *Sensors* **2008**, *8*, 1400–1458.
7. Brecht, A.; Gauglitz, G.; Nahm, W. Interferometric Measurements Used in Chemical and Biochemical Sensors. *Analysis* **1992**, *20*, 135–140.
8. Lin, V. S.-Y.; Motesharei, K.; Dancil, K. S.; Sailor, M. J.; Ghadiri, M. R. A Porous Silicon-Based Optical Interferometric Biosensor. *Science* **1997**, *278*, 840–843.
9. Dancil, K.-P. S.; Greiner, D. P.; Sailor, M. J. A Porous Silicon Optical Biosensor: Detection of Reversible Binding of IgG to a Protein A-Modified Surface. *J. Am. Chem. Soc.* **1999**, *121*, 7925–7930.
10. Meskini, O.; Abdelghani, A.; Tlili, A.; Mgaieth, R.; Jaffrezic-Renault, N.; Martelet, C. Porous Silicon as Functionalized Material for Immunosensor Application. *Talanta* **2007**, *71*, 1430–1433.
11. Schwartz, M. P.; Alvarez, S. D.; Sailor, M. J. A Porous SiO_2 Interferometric Biosensor for Quantitative Determination of Protein Interactions: Binding of Protein A to Immunoglobulins Derived from Different Species. *Anal. Chem.* **2007**, *79*, 327–334.
12. Pacholski, C.; Yu, C.; Miskelly, G. M.; Godin, D.; Sailor, M. J. Reflective Interferometric Fourier Transform Spectroscopy: A Self-Compensating Label-Free Immunosensor Using Double-Layers of Porous SiO_2. *J. Am. Chem. Soc.* **2006**, *128*, 4250–4252.
13. Bonanno, L. M.; DeLouise, L. A. Whole Blood Optical Biosensor. *Biosens. Bioelectron.* **2007**, *23*, 444–448.
14. Pan, S.; Rothberg, L. J. Interferometric Sensing of Biomolecular Binding Using Nanoporous Aluminum Oxide Templates. *Nano Lett.* **2003**, *3*, 811–814.
15. Casanova, F.; Chiang, C. E.; Li, C.-P.; Roshchin, I. V.; Ruminski, A. M.; Sailor, M. J.; Schuller, I. K. Effect of Surface Interactions on the Hysteresis of Capillary Condensation in Nanopores. *Europhys. Lett.* **2008**, *81*, 26003.
16. Lau, K. H. A.; Tan, L. S.; Tamada, K.; Sander, M. S.; Knoll, W. Highly Sensitive Detection of Processes Occurring inside Nanoporous Anodic Alumina Templates: A Waveguide Optical Study. *J. Phys. Chem. B* **2004**, *108*, 10812–10818.
17. Masuda, H.; Yamada, H.; Satoh, M.; Asoh, H.; Nakao, M.; Tamamura, T. Highly Ordered Nanochannel-Array Architecture in Anodic Alumina. *Appl. Phys. Lett.* **1997**, *71*, 2770–2772.
18. Briggs, E. P.; Walpole, A. R.; Wilshaw, P. R.; Karlsson, M.; Pålsgård, E. Formation of Highly Adherent Nano-Porous Alumina on Ti-Based Substrates: A Novel Bone Implant Coating. *J. Mater. Sci.: Mater. Med.* **2004**, *15*, 1021–1029.
19. Orosco, M. M.; Pacholski, C.; Miskelly, G. M.; Sailor, M. J. Protein-Coated Porous Silicon Photonic Crystals for Amplified Optical Detection of Protease Activity. *Adv. Mater.* **2006**, *18*, 1393–1396.
20. Yamaguchi, A.; Hotta, K.; Teramae, N. Optical Waveguide Sensor Based on a Porous Anodic Alumina/Aluminum Multilayer Film. *Anal. Chem.* **2009**, *81*, 105–111.
21. Segal, E.; Perelman, L. A.; Cunin, F.; Di Renzo, F.; Devoisselle, J. M.; Li, Y. Y.; Sailor, M. J. Confinement of Thermoresponsive Hydrogels in Nanostructured Porous Silicon Dioxide Templates. *Adv. Funct. Mater.* **2007**, *17*, 1153–1162.
22. Huber, K. Pore Volume of Electrolytically Produced Protective Coatings on Aluminum. *J. Colloid Sci.* **1948**, *3*, 197–206.
23. Saphire, E. O.; Parren, P. W. H. I.; Barbas III, C. F.; Burton, D. R.; Wilson, I. A. Crystallization and Preliminary Structure Determination of an Intact Human Immunoglobulin, B12: An Antibody That Broadly Neutralizes Primary Isolates of HIV-1. *Acta Crystallogr., Sect. D* **2001**, *57*, 168–171.
24. Casanova, F.; Chiang, C. E.; Li, C.-P.; Roshchin, I. V.; Ruminski, A. M.; Sailor, M. J.; Schuller, I. K. Gas Adsorption and Capillary Condensation in Nanoporous Alumina Films. *Nanotechnology* **2008**, *19*, 315709.
25. Collins, B. E.; Dancil, K.-P.; Abbi, G.; Sailor, M. J. Determining Protein Size Using an Electrochemically Machined Pore Gradient in Silicon. *Adv. Funct. Mater.* **2002**, *12*, 187–191.
26. Canham, L. T. Bioactive Silicon Structure Fabrication through Nanoetching Techniques. *Adv. Mater.* **1995**, *7*, 1033–1037.
27. Canham, L. T.; Reeves, C. L.; Newey, J. P.; Houlton, M. R.; Cox, T. I.; Buriak, J. M.; Stewart, M. P. Derivatized Mesoporous Silicon with Dramatically Improved Stability in Simulated Human Blood Plasma. *Adv. Mater.* **1999**, *11*, 1505–1507.
28. Sohn, H.; Létant, S.; Sailor, M. J.; Trogler, W. C. Detection of Fluorophosphonate Chemical Warfare Agents by Catalytic

Hydrolysis with a Porous Silicon Interferometer. *J. Am. Chem. Soc.* **2000**, *122*, 5399–5400.
29. Steinem, C.; Janshoff, A.; Lin, V. S. Y.; Völcker, N. H.; Reza Ghadiri, M. DNA Hybridization-Enhanced Porous Silicon Corrosion: Mechanistic Investigations and Prospect for Optical Interferometric Biosensing. *Tetrahedron* **2004**, *60*, 11259–11267.
30. Voelcker, N. H.; Alfonso, I.; Ghadiri, M. R. Catalyzed Oxidative Corrosion of Porous Silicon Used as an Optical Transducer for Ligand−Receptor Interactions. *ChemBioChem* **2008**, 1776–1786.
31. Jiang, J.; Huo, K.; Wu, Z.; Chen, S.; Pu, S.; Yu, Z.; Liu, X.; Chu, P. K. Silicon-Induced DNA Damage Pathway and Its Modulation by Titanium Plasma Immersion Ion Implantation. *Biomaterials* **2008**, *29*, 544–550.
32. Van Gestel, T.; Vandecasteele, C.; Buekenhoudt, A.; Dotremont, C.; Luyten, J.; Leysen, R.; Van der Bruggen, B.; Maes, G. Alumina and Titania Multilayer Membranes for Nanofiltration: Preparation, Characterization and Chemical Stability. *J. Membr. Sci.* **2002**, *207*, 73–89.
33. Harlow, E.; Lane, D. *Antibodies: A Laboratory Manual*; Cold Spring Harbor Laboratory: Cold Spring Harbor, NY, 1988; p 726.
34. Langone, J. J. Protein A of *Staphylococcus aureus* and Related Immunoglobulin Receptors Produced by Streptococci and Pneumonococci. In *Advances in Immunology*; Academic Press: New York, 1982; Vol. 32, pp 157−252.
35. David, H.; Gordon, L.; Robert, B.; Flynn, T. G. Protein Immobilization to Alumina Supports: I. Characterization of Alumina-Organophosphate Ligand Interactions and Use in the Attachment of Papain. *Biotechnol. Bioeng.* **1992**, *40*, 1319–1327.
36. Djokic, S. S.; Burrell, R. E. Visual Detection of Protein Adsorption onto Electrochemically Oxidized Aluminum Surfaces. *Biosens. Bioelectron.* **1998**, *13*, 271–278.
37. Cheow, P. S.; Liu, L. Y.; Toh, C. S. Grafting of Nanoporous Alumina Membranes and Films with Organic Acids. *Surf. Interface Anal.* **2007**, *39*, 601–610.
38. Malmsten, M. Ellipsometry Studies of the Effects of Surface Hydrophobicity on Protein Adsorption. *Colloids Surf., B* **1995**, *3*, 297–308.
39. Schwartz, M. P.; Yu, C.; Alvarez, S. D.; Migliori, B.; Godin, D.; Chao, L.; Sailor, M. J. Using an Oxidized Porous Silicon Interferometer for Determination of Relative Protein Binding Affinity through Non-Covalent Capture Probe Immobilization. *Phys. Status Solidi A* **2007**, *204*, 1444–1448.
40. Gutenwik, J.; Nilsson, B.; Axelsson, A. Effect of Hindered Diffusion on the Adsorption of Proteins in Agarose Gel Using a Pore Model. *J. Chromatogr., A* **2004**, *1048*, 161–172.
41. Popat, K. C.; Mor, G.; Grimes, C. A.; Desai, T. A. Surface Modification of Nanoporous Alumina Surfaces with Poly(ethylene glycol). *Langmuir* **2004**, *20*, 8035–8041.
42. Cheow, P.-S.; Liu, L.; Toh, C. S. Grafting of Nanoporous Alumina Membranes and Films with Organic Acids. *Surf. Interface Anal.* **2007**, *39*, 601–610.
43. Leary Swan, E. E.; Popat, K. C.; Desai, T. A. Peptide-Immobilized Nanoporous Alumina Membranes for Enhanced Osteoblast Adhesion. *Biomaterials* **2005**, *26*, 1969–1976.
44. Vlassiouk, I.; Krasnoslobodtsev, A.; Smirnov, S.; Germann, M. "Direct" Detection and Separation of DNA Using Nanoporous Alumina Filters. *Langmuir* **2004**, *20*, 9913–9915.